Title:

A chromosome-scale *Lotus japonicus* Gifu genome assembly indicates that symbiotic islands are not general features of legume genomes

Authors:

Nadia Kamal[1], Terry Mun[2], Dugald Reid[2], Jie-shun Lin[2], Turgut Yigit Akyol[3], Niels Sandal[2], Torben Asp[2], Hideki Hirakawa[4], Jens Stougaard[2], Klaus F. X. Mayer[1,5], Shusei Sato[3], and Stig Uggerhøj Andersen[2]

Author affiliations:

1: Helmholtz Zentrum München, German Research Center for Environmental Health, Plant Genome and Systems Biology, Ingolstädter Landstr. 1, 85764 Neuherberg, Germany.

2: Department of Molecular Biology and Genetics, Aarhus University, Gustav Wieds Vej 10, DK-8000 Aarhus C, Denmark.

3: Graduate School of Life Sciences, Tohoku University, 2-1-1 Katahira, Aoba-ku, Sendai, 980-8577, Japan

4: Kazusa DNA Research Institute, 2-1-1 Kazusa-Kamatari, Kisarazu, Chiba, 292-0816, Japan

5: Technical University Munich, Munich Germany

Authors for correspondence:

Klaus F. X. Mayer (k.mayer@helmholtz-muenchen.de), Shusei Sato (shuseis@ige.tohoku.ac.jp), and Stig U. Andersen (sua@mbg.au.dk)

Abstract

Lotus japonicus is a herbaceous perennial legume that has been used extensively as a genetically tractable model system for deciphering the molecular genetics of symbiotic nitrogen fixation. So far, the *L. japonicus* reference genome assembly has been based on Sanger and Illumina sequencing reads from the *L. japonicus* accession MG-20 and contained a large fraction of unanchored contigs. Here, we use long PacBio reads from *L. japonicus* Gifu combined with Hi-C data and new high-density genetic maps to generate a high-quality chromosome-scale reference genome assembly for *L. japonicus*. The assembly comprises 554 megabases of which 549 were assigned to six pseudomolecules that appear complete with telomeric repeats at their extremes and large centromeric regions with low gene density. The new *L. japonicus* Gifu reference genome and associated expression data represent valuable resources for legume functional and comparative genomics. Here, we provide a first example by showing that the symbiotic islands recently described in *Medicago truncatula* do not appear to be conserved in *L. japonicus*.

Introduction

Lotus japonicus (*Lotus*) is a well-characterized perennial legume widely used because of its short generation time, abundant flowers, small diploid genome, amenability to tissue culture and *Agrobacterium* transformation, self-compatibility, and inter- and intra-specific fertility enabling genetic mapping [1-4]. Due to its ability to participate in both nitrogen fixing symbiosis with rhizobia and symbiosis with arbuscular mycorrhiza [5], *Lotus* has played a key role in developing our current understanding of the molecular mechanisms behind root nodule development and symbiotic nitrogen-fixation [6-8] and arbuscular mycorrhizal symbiosis [9-11].

The genetic tools available in *Lotus* include EMS mutants [12], sequenced sets of wild accessions [13] and recombinant inbred lines [4,14,15] as well as extensive populations of TILLING lines [16] and *LORE1* insertion mutants [17-19]. Last, but not least, large volumes of biological data generated using *Lotus*, such as expression studies that describe responses to environmental cues and symbionts and pathogens [20-30], and data from more than 700,000 unique *LORE1* insertions found in more than 130,000 mutant lines [18], have been integrated in an online portal known as *Lotus* Base [31], available from https://lotus.au.dk. This online portal provides researchers a one-stop resource for *Lotus* data retrieval, visualization, interrogation, and analysis.

Lotus has a relatively small genome size estimated to ~500 Mb [32]. Three major sequencing and assembly efforts have been performed using the *Lotus* accession MG-20. MG-20 was selected due to its early, abundant flowering phenotype, and ability to sustain robust growth under both growth chamber and greenhouse conditions [33]. For clone-by-clone sequencing of the *Lotus* genome, genomic clones, constructed mainly using a TAC (Transformation-competent Artificial Chromosome) vector, were selected based on expressed sequence tag (EST) sequence information as seed points of the gene-rich genome regions. The nucleotide sequence of each clone was determined using a shotgun sequencing strategy with 10 times redundancy, and the sequenced clones were anchored onto six chromosomes using a total of 788 microsatellite markers. In parallel with the clone-by-clone approach, shotgun sequencing of selected genomic regions was carried out using two types of

shotgun libraries, a random genomic library from which highly repetitive and organelle genomic sequences were subtracted and a shotgun library constructed from a mixture of 4,603 TAC clones selected from unsequenced gene space, with the aim to accumulate draft sequence information for the remaining gene rich regions. In the first report of the genome sequence of *Lotus* MG-20 (version 1.0 in 2008) [34], a total of 1,898 TAC/BAC clones were sequenced and assembled into 954 supercontigs with a total length of 167 Mbp, of which 130 Mbp were anchored onto 6 chromosomes. In combination with draft assembly of shotgun sequences from selected genomic regions, the total length of the v. 1.0 assembly was 315 Mbp. While this assembly corresponded to 67% of the reported *Lotus* genome (472 Mb) [32], it was estimated that it covered ~91 % of the gene space because 11,404 out of 12,485 tentative consensus (TC) sequences of the *Lotus* Gene Index provided by the Gene Index Project could be mapped to the v1.0 assembly. In 2010, an updated genome sequence, v2.5, was constructed by adding genome sequence information from 460 TAC/BAC clones analyzed after the release of v1.0, increasing the total length of anchored contigs to 195 Mbp. This Sanger-based sequence information is currently available at http://www.kazusa.or.jp/lotus/build2.5.

With the advent of high-throughput and low cost next-generation sequencing (NGS) technology, the strategy for genome sequencing changed from clone-by-clone Sanger sequencing to whole-genome shotgun approaches. In 2009, the NGS shotgun approach was implemented in the *Lotus* genome sequencing project using two emerging NGS platforms, 454 GS FLX and Illumina. Since there was no assembly program available that could carry out hybrid assembly of short reads from NGS and longer Sanger-based contigs, a step-by-step approach for combined assembly was used. The accumulated Illumina reads were used to create a de novo assembly using the assembler SOAPdenovo 1.04 [35], and the obtained contigs were applied to the hybrid assembly with the phase1 draft sequence clones and selected genome assembly contigs in v2.5 by using the assembly program PCAP.rep [36]. After the phase 2 and phase 3 clone sequences in v2.5 were integrated into the resulting hybrid contigs, scaffolding of the contigs was carried out by applying paired-end reads of the genomic DNA from the GS FLX sequencer and end sequences of TAC and BAC clones. The resulting sequence from this hybrid assembly approach was released as version 3.0 of the *Lotus*

MG-20 genome. In this assembly, a total of 132 scaffolds covering 232 Mbp of the genome were aligned to the six *Lotus* chromosomes. The total number of scaffolds was thus decreased to one-fifth from 646 scaffolds in v2.5, and the total length of anchored contigs increased by 20% from 195 Mbp in v2.5. The remaining 23,572 unanchored contigs, corresponding to 162 Mbp were assigned to a virtual chromosome 0. The gene space coverage of v3.0 was estimated to be ~98% based on the mapping of 57,916 de novo assembled RNA-seq contigs. The MG-20 version 3.0 data is available from Lotus Base (https://lotus.au.dk/) [31] and the Kazusa DNA Research Institute database (https://www.kazusa.or.jp/lotus/).

The establishment of a large insertion mutant population — almost 140,000 unique lines — using a de-repressed endogenous retrotransposon known as *LORE1* in a *Lotus* ecotype Gifu (accession B-129) background [17-19,37] necessitates an assembled genome of the same genetic background with predicted transcripts and proteins. All previous *Lotus* sequencing efforts performed in *Lotus* were exclusively in an MG-20 background, which is known to differ from the Gifu genome due to translocation events [33,38,39].

Medicago truncatula (*Medicago*) is the other main legume model for symbiotic nitrogen fixation [40]. Recently, a high quality assembly of the *Medicago truncatula* accession A17 was published, and a comprehensive gene expression study led to the identification of "symbiotic islands", representing clusters of genes that showed co-regulated, symbiosis-related expression profiles [41]. Interestingly, these clusters were rich in long non-coding (lnc) RNAs, and it was speculated that the lncRNAs may be involved in regulating symbiosis-related gene expression.

Here, we present a high-quality *Lotus* Gifu reference assembly constructed based on 100x PacBio read coverage and scaffolded using Hi-C and genetic map data. We use this high-quality assembly to explore the positional clustering of putative orthologs of *Medicago* lncRNAs and compare nodule-regulated gene-clusters designated "Nodule upregulated (NRU)", "Nodule downregulated (NRD)" and "Nodule non-regulated (NRN)" between *Lotus* and *Medicago.* Conserved gene regulation was found for root and nodule samples although evidence supporting conservation of the symbiotic islands discovered in *Medicago* did not emerge.

Results

A chromosome-scale *Lotus* Gifu assembly including telo- and centromeric repeats

We generated a total of 11.8 million PacBio RSII reads, which we assembled using Canu [42] into 1686 contigs with an N50 of 807 kb and a total length of 554 Mb (**Table 1**). We first scaffolded the contigs using 175 million Proximo Hi-C reads (Phase genomics). To validate the scaffolding, we mapped whole genome re-sequencing data from two recombinant inbred line populations [15] to the PacBio contigs. The vast majority of the assembly, 99.5%, was contained within contigs that had at least one polymorphic SNP marker, leaving only 2.5 Mb of sequence on markerless contigs (**Table 2**). We compared the Hi-C scaffolding results to the genetic maps generated based on the recombinant inbred line data (**Supplemental file 1**) and moved contigs according to genetic linkage. We then repeated the scaffolding until the Proximo Hi-C results were concordant with the genetic maps and the contigs were arranged in six pseudomolecules corresponding to the six *Lotus* chromosomes (**Supplemental file 2**). The total length of the assembly was close to the expected genome size of ~500 Mb (**Table 1**), and we found canonical telomeric repeats at the ends of all pseudomolecules, except for the bottom of chromosome three, indicating a high completeness of the assembly. The 2.5 Mb of unanchored contigs placed on chr0 contained a substantial amount of pericentromeric repeats.

Regarding the highly repetitive sequences, three 45S rDNA clusters and a 5S rDNA gene cluster were anchored on chromosomes 2, 5 and 6, and on chromosome 2, respectively, consistent with FISH data (**Figure 1A**) [38]. In addition to the regions with high density of repetitive sequences, corresponding to the pericentromeric regions of each chromosome, small regions with high densities of repetitive sequences were identified within the gene rich regions of the bottom arm of chromosomes 2 and 4 (**Figure 1A**). The location of these regions corresponded to the positions of chromosome knobs reported in the previous cytological analyses [38,43]. These regions with highly dense repetitive sequences tend to be composed of contigs with short length, and thus a significant number of the sequence gaps (389 out of 1555) were found in these regions. Despite the relatively

high frequency of sequence gaps in these repetitive regions, the Hi-C reads provided sufficient physical linking information to allow scaffolding.

Genome annotation

Based on evidence from expression data as well as homology information from related species, 30,243 genes were annotated, 21,778 of which represent high confidence gene models (**Table 3, Supplemental file 3**). Using the embryophyta_odb10 lineage 1,584 out of 1,614 (98.2%) complete BUSCO v4 orthologs [44] were found in the genome assembly and 1,551 (96.1%), were identified within the annotated gene set (**Figure 1B**). The high confidence gene set had a BUSCO score of 94%. Using AHRD [45] we could assign functional annotations to 29,429 genes (97%). Of these, 70.53% fulfilled all three AHRD quality criteria, 16.85% fulfilled two and 11.8% fulfilled one criterion. We then annotated non-coding RNAs, identifying 2,933 in total that comprised 128 micro RNAs, 851 snoRNAs, 88 tRNAs, 795 rRNAs and others. In total, gene models covered 156,379,918 bases and coding exons covered 60,649,299 bases of the genome assembly.

Repetitive elements made up 260,312,827 bases (46.96 %) of the genome. Of these, long terminal repeat retrotransposons accounted for most of the repeat content of the genome (42.51%), followed by DNA transposons and low complexity regions (**Figure 1C**). Chromosomes 1, 3, 4, 5, and 6 showed centrally located pericentromeric regions rich in repetitive elements flanked by gene-rich regions (**Figure 1A**). In contrast, the centromere of chromosome 2 appeared to be distally located near the top of the chromosome, which also carried a large cluster of rRNA genes (**Figure 1A**).

RNA-seq based expression atlas

To produce a gene expression atlas, publicly available RNA-seq data from *Lotus* Gifu was obtained for 35 conditions across different tissues, symbiotic and pathogenic interactions (Accession numbers available in **Supplemental table 1**). The conditions available include root hair, nodule primordia and nodules obtained after inoculation with *Mesorhizobium loti* R7A and root interactions with microbes across a symbiont-pathogen spectrum (Kelly et al 2018); root and shoot tissues three days after roots were inoculated with *M. loti* (Munch et al., 2107); root symbiotic susceptible zone treated with

cytokinin (1 μM BA) or *M. loti* R7A (this study); roots inoculated with the arbuscular mycorrhizal fungus (AMF), *Glomus intratadices* (Handa et al 2015); root, leaf, immature flowers, mature flowers, pods and seeds (National Institute for Basic Biology, 2016). Gene-level quantification of the data was normalised across conditions (**Supplemental file 4**) and is made available through Lotus Base (https://lotus.au.dk/expat/) to provide a readily accessible expression viewer. Well-described nodulation genes, including *Nin*, *CCamK* and *Cyclops* [46-48], showed the expected expression patterns across the conditions represented in the expression atlas (**Figure 2**).

Symbiotic islands are not generally conserved between *Lotus* and *Medicago*

To investigate if the symbiotic islands recently described in *Medicago* [41] were conserved in *Lotus*, we extracted the best Lotus BLAST hits against the *Medicago* genes reported to reside within symbiotic islands (**Supplemental file 5**). Protein coding genes were generally well conserved and showed high levels of microsynteny, regardless of whether or not they were present in gene islands that showed symbiosis-related differential expression (**Table 4**). Out of 760 islands, 266 had at least three distinct *Lotus* hits in microsyntenic regions, and the region with the largest overlap comprised 12 hits. In contrast, most *Medicago* lncRNAs had no putative orthologs in the *Lotus* genome, and, when identified, they were often not found within the designated microsyntenic region (**Table 4**). Across all 760 investigated islands, a total of six had two lncRNA hits to the *Lotus* microsyntenic region, and no island had more than two.

The limited conservation and lack of positional clustering make it unlikely that putative orthologs of *Medicago* lncRNAs are generally part of symbiotic islands in *Lotus*. Instead, we looked further into the protein coding genes to determine if their organisation into symbiotic islands could be conserved. All 760 islands contain at least one protein coding gene. Out of these, we examined the 443 islands associated with nodule-regulated genes designated “Nodule upregulated (NRU)”, “Nodule downregulated (NRD)” and “Nodule non-regulated (NRN)”. First, we investigated the level of expression conservation by comparing the expression of *Medicago* genes in symbiotic islands and their *Lotus* syntenic homologs in root and 10 dpi nodule samples (**Supplemental tables 1-2 and**

Supplemental files 4 and 6). The genes associated with *Medicago* NRU islands showed strongly correlated expression responses in *Lotus* and *Medicago*, NRD genes showed a less pronounced correlation, while there was no correlation for the NRN genes (**Figure 3A**).

To quantify the level of co-regulation within putative symbiotic islands, we calculated the average Pearson correlation coefficients for each island based on the gene expression data from root and nodule samples (**Supplemental tables 1-2**). First, we included all genes in *Medicago* symbiotic islands that had a *Lotus* BLAST match anywhere in the genome along with their best *Lotus* match. If a *Lotus* gene was the best match for multiple *Medicago* genes, it was included multiple times in the analysis. Especially for the NRU islands, this resulted in a very pronounced skew towards high correlation coefficients as compared to the NRN islands, and this was true both for *Lotus* and *Medicago* (**Figure 3B**).

We then repeated the analysis including only Medicago-*Lotus* syntenic homolog pairs from islands with at least three unique *Lotus* genes. That is, if multiple *Medicago* genes matched the same *Lotus* gene, only a single *Medicago* gene was retained and each unique *Lotus* gene was only included once per island. This resulted in a marked reduction in the number of islands and the large peak of near perfect correlation coefficients for NRU islands disappeared for both *Lotus* and *Medicago* (**Figure 3C**). Since there was no longer a major difference between the root/nodule-based correlation coefficients between the nodule-regulated NRU and NRD islands and the NRN controls, it appears that local gene amplification in *Medicago* is a major cause of the symbiotic island signal. This is consistent with an overall high ratio of *Medicago* to *Lotus* genes in symbiotic islands (**Table 4**). Symbiotic islands are thus not generally conserved between *Lotus* and *Medicago* and are not general features of legume genomes. However, we did find a few examples of gene clusters that showed conserved co-regulation for root and nodule samples (**Supplemental tables 3-5**). In *Lotus*, NRU island SRI_NDD0105, which had the second highest *Lotus* correlation coefficient (**Supplemental table 3**), had three very similar copies of a nodulin gene, suggesting that local gene amplification also plays a role here. In contrast, the NRU island with the highest *Lotus* correlation

coefficient (SRI_NRU0026) comprised three very different genes, perhaps warranting further investigation (**Supplemental table 3**).

Discussion

By applying long PacBio reads, the contiguity of the assembly was improved compared to the MG-20 version 2.5 assembly that was a hybrid assembly based on Sanger and Illumina sequences. Using Hi-C paired-end reads and high-density SNP marker information generated by re-sequencing of *L. burttii* x *L. japonicus* Gifu RILs, 1584 contigs were anchored onto 6 chromosomes with 42 scaffolds, providing a high-quality and well-validated assembly. The number of scaffolds was a bit larger than that of the latest A107 sequence (Mt5.0) due to manual correction of Hi-C scaffolding errors based on the SNP marker information. Typical Hi-C scaffolding errors were identified in the distal regions of each pseudomolecule and at the border regions of chromosome knobs located on chromosomes 2 and 4, presumably due to an atypical three-dimensional chromosome conformation in those regions. A total of 30,243 high and low confidence gene models were annotated, which corresponds approximately to the number of high confidence gene models in the *Medicago* v. 4 assembly (**Table 3**). The total number of annotated genes is higher for *Medicago* versions 4 and 5 than for the current *Lotus* Gifu assembly. However, the number of exons per transcript is markedly lower for the full *Medicago* gene sets than for the *Lotus* gene and *Medicago* v.4 high confidence gene sets, suggesting that the differences in gene numbers are due to different stringencies in including small genes with few exons. As expected, the paleopolyploid *Glycine max* [49] has a higher number of annotated genes than *Lotus* but retains a similar exon per transcript ratio despite more than 50,000 annotated genes.

The availability of a high-quality *Lotus* Gifu assembly will facilitate further improvements of genetic and genomic *Lotus* resources. The *LORE1* mutant collection, which includes more than 130,000 insertion mutant lines, is in the Gifu genetic background, but was annotated based on the MG-20 v. 2.5 assembly [17-19]. Using the new Gifu sequence, the *LORE1* insertions can now be more accurately characterised. Likewise, Gifu is more closely related to the majority of the collection of wild *Lotus*

accessions that was recently characterized [13], and the new reference assembly should allow an improved characterization of the genetic diversity. Here, we have mapped existing and new RNA-seq data to the Gifu assembly to provide a consistently normalized and updated *Lotus* gene expression atlas readily available through *Lotus Base* [31]. The current atlas does not comprise as many samples as previously profiled using microarrays [24,30], but it is not limited by probe set selection and has data on all annotated and expressed genes.

Here, the new assembly and expression atlas have also proved useful in interspecific comparisons, since the complete pseudomolecules allowed us to accurately assess synteny with *Medicago* to investigate the level of conservation of plant symbiotic islands. Interestingly, the recently identified *Medicago* symbiotic islands did not appear to be conserved in *Lotus*. This was most evident for the *Medicago* non-coding RNAs, for which we could find only very few matching sequences in *Lotus* despite the completeness of the assembly. It should be noted that many of the transcripts classified as long non-coding RNAs in the *Medicago* study [41] in fact encode peptides, most notably the large family of nodule cysteine-rich (NCR) peptides. The NCR peptides are characteristic of the Inverted Repeat Lacking Clade (IRLC) legume lineage and thus not found in *Lotus* [50]. The same appears to be the case for the other transcripts in the non-coding class, indicating that non-coding and peptide-encoding genes have evolved rapidly and are not generally required for legume-rhizobium symbiosis across determinate and indeterminate nodulators.

For the protein coding genes in symbiotic islands, we found much higher levels of conservation and microsynteny, but most of the local co-regulation appeared to be related to tandem gene duplications in *Medicago*. Generally, *Medicago* seems to have experienced not only a rapid expansion of NCR peptide genes and lncRNAs involved in symbiosis, but also of protein coding genes with symbiosis-related expression patterns, and our results clearly indicate that symbiotic islands are not general features of legume genomes.

Materials and Methods

PacBio data generation and assembly

L. japonicus Gifu high-molecular weight DNA was extracted as described [51] and sent to Earlham Institute and Takara Bio Inc. for PacBio sequencing. A total of 5.45 million reads with an average length of 8 kb were generated. The PacBio reads were assembled using Canu (v1.3) [42] with the parameters corOutCoverage=100 errorRate=0.015 corMhapSensitivity=normal corMaxEvidenceErate=0.15 oeaMemory=15 cnsMemory=40. The assembled contigs were then polished using PacificBiosciences' GenomicConsensus package using Quiver (https://github.com/PacificBiosciences/GenomicConsensus).

Constructing genetic maps based on data from two RIL populations

Paired-end reads from recombinant inbred lines (RILs) of Gifu×*L. burttii* and Gifu×MG-20, as well as those from their respective parental lines (*L. japonicus* Gifu, *L. japonicus* MG-20, and *L. burttii*), were mapped to the polished assembly using BWA-MEM [52]. Picard (http://broadinstitute.github.io/picard/) was used to dedupe the generated BAM files, followed by variant calling using mpileup provided by SAMtools [53]. The resulting VCF files were filtered based on the following criteria: (1) minimum quality of 30, (2) minimum depth of 50, (3) must be biallelic, and (4) cannot contain missing genotypes. To further improve the quality of the genetic map, further filtering was performed using a Python script to select solely for single nucleotide polymorphisms (SNPs) that are homozygous in the Gifu parent and homozygous alternative in the second RIL parent (*L. japonicus* MG-20 or *L. burttii*). Out of the 1,686 contigs present in the preliminary Gifu genome assembly, 148 do not contain any SNPs. Of the remaining 1,538 contigs that contain at least one or more SNPs from either RIL populations, 105 contain SNPs derived exclusively from the Gifu×*L. burttii* RIL population and 124 from the Gifu×MG-20 RIL population. The remaining 1,309 contigs have SNPs derived from both populations (**Table 1**). SNPs appears to be well-distributed in the genome, with a large majority of contigs (77.6%) containing at least one SNP from both populations constituted by 97.9% of the bases.

A genetic map is constructed to aid the assembly and scaffolding of the preliminary Gifu assembly. To generate a consensus genotype call pattern for each contig across each RIL population (Gifu × *L. burttii* and Gifu×MG-20), the most commonly occurring genotype across all positions was selected. A confidence score was assigned to each RIL within the population, and an average confidence score (on a per contig basis across the entire population) was then calculated.

Assembly scaffolding based on genetic maps and Hi-C data

Gifu leaf tissue was sent to Phase Genomics (https://phasegenomics.com), where Hi-C sequencing was carried out and a draft proximity-based (Proximo) scaffolding generated.

Chromatin conformation capture data was generated using a Phase Genomics (Seattle, WA) Proximo Hi-C [54]. Intact cells from two samples were crosslinked using a formaldehyde solution, digested using the Sau3AI restriction enzyme, and proximity ligated with biotinylated nucleotides to create chimeric molecules composed of fragments from different regions of the genome that were physically proximal in vivo, but not necessarily genomically proximal. Molecules were pulled down with streptavidin beads and processed into an Illumina-compatible sequencing library. Sequencing was performed on an Illumina NextSeq 500, generating a total of 175,495,827 PE150 read pairs.

Reads were aligned to the draft PacBio assembly scaffoldSeq.fasta using bwa mem with the -5 option [52]. Alignments were then filtered with samtools [53] using the -F 2316 filtering flag.

Phase Genomics' Proximo Hi-C genome scaffolding platform was used to create chromosome-scale scaffolds from the draft assembly in a method similar to that described by Bickhart et al. [55]. As in the LACHESIS method [56], this process computes a contact frequency matrix from the aligned Hi-C read pairs, normalized by the number of Sau3AI restriction sites (GATC) on each contig, and constructs scaffolds in such a way as to optimize expected contact frequency and other statistical patterns in Hi-C data. Approximately 88,000 separate Proximo runs were performed to optimize the number of scaffolds and scaffold construction in order to make the scaffolds as concordant with the observed Hi-C data as possible. This process resulted in a set of six chromosome-scale scaffolds containing 549 Mbp of sequence (>99% of the draft assembly).

Chimeric contigs were identified based on genetic map, Hi-C, and PacBio coverage data and split. The initial scaffolding was then iteratively improved using genetic map data followed by re-running Proximo scaffolding until genetic map and proximity-based scaffolding results converged.

Annotation of protein coding genes

The annotation of the *Lotus* Gifu genome was performed using evidence from transcriptome data as well as homology information from related species. For the homology-based annotation, available *Arabidopsis thaliana* (Araport11), *Glycine max* (v2.1) and *Medicago* (MtrunA17r5.0-ANR) protein sequences were combined. These protein sequences were mapped to the *Lotus* Gifu genome sequence v1.2 using the splice-aware alignment tool GenomeThreader [57] (version 1.6.6; with the arguments -startcodon -finalstopcodon -species rice -gcmincoverage 70 -prseedlength 7 -prhdist 4). In the expression data-based step, multiple RNA-seq datasets (SRP127678, SRP105404, DRP000629, PRJNA622801) were used as evidence for the genome-guided prediction of gene structures. Therefore, reads from RNA-seq datasets were mapped to the genome using Hisat2 (version 2.1, parameter –dta) [58] and subsequently assembled into transcript sequences with Stringtie (version 1.2.3, parameters -m 150 -t -f 0.3) [59]. Next, Transdecoder (version 3.0.0) (https://github.com/TransDecoder/TransDecoder) was used to identify potential open reading frames and predict protein sequences. Using BLASTP (ncbi-blast-2.3.0+, parameters -max_target_seqs 1 -evalue 1e-05) [60] the predicted protein sequences were compared against a protein reference database (Uniprot Magnoliophyta, reviewed/Swissprot) and used hmmscan (version 3.1b2) [61] to identify conserved protein family domains for all proteins. BLAST and hmmscan results were then used by Transdecoder-predict and the best translations per transcript sequence was selected. Finally, results from the two gene prediction approaches were combined and redundant protein sequences were removed. Additionally, some symbiosis genes were manually curated (**Supplemental table 6**).

In order to classify gene models into complete and functional genes, non-coding transcripts, pseudogenes and transposable elements, a confidence classification protocol was applied.

Candidate protein sequences were compared against the following three databases using BLAST: PTREP, a manually curated database of hypothetical proteins that contains deduced protein sequences, from which frameshifts have mostly been removed (http://botserv2.uzh.ch/kelldata/trep-db/index.html). A database with annotated proteins from the legumes *Glycine max* and *Medicago* (Fab); and, UniMag a database of validated proteins from the Magnoliophyta. UniMag protein sequences were downloaded from Uniprot and further filtered for complete sequences with start and stop codons. Best hits were selected for each predicted protein to each of the three databases. Only hits with an E-value below 10e-10 were considered. Furthermore, only hits with subject coverage above 80% were considered significant and protein sequences were further classified into high and low confidence. High confidence (HC) protein sequences are complete and have a subject and query coverage above the threshold in the UniMag database (HC1) or no blast hit in UniMag but in Fab and not PTREP (HC2). While a low confidence (LC) protein sequence is not complete and has a hit in the UniMag or Fab database but not in PTREP (LC1), or no hit in UniMag and Fab and PTREP but the protein sequence is complete.

Functional annotation

Functional annotation of transcripts as well as the assignment of GO terms was performed using the tool "Automatic assignment of Human Readable Descriptions - AHRD". AHRD performs BLASTP search against Swissprot, Tair and Trembl databases to perform functional annotation based on homology to other known proteins and integrates domain search results from InterProScan as well as gene ontology (GO) terms [45].

Repeat annotation and prediction of ncRNAs

Repeats were annotated using Repeatmasker (Smit, AFA, Hubley, R & Green, P. RepeatMasker Open-4.0.2013-2015 <http://www.repeatmasker.org>) version 3.3 with a custom Fabaceae-library in sensitive mode. Non-coding RNAs were predicted using tRNAscan-SE (version 1.3.1) [62], RNAmmer (version 1.2) [63] and Infernal (version 1.1.2) [64] with default parameters. The results were merged subsequently.

Expression atlas

Raw *L. japonicus* Gifu RNA-seq reads were obtained from Sequence Read Archive (SRA) for the listed accessions (**Supplemental table 1**). A decoy-aware index was built for Gifu transcripts using default Salmon parameters and reads were quantified using the --validateMappings flag [65] (Salmon version 0.14.1). A normalised expression atlas across all conditions was constructed using the R-package DESeq2 version 1.20 [66] after summarising gene level abundance using the R-package tximport (version 1.8.0). Normalised count data obtained from DESeq2 are available in the *Lotus* Base expression atlas (https://lotus.au.dk/expat/) [31].

Analysis of symbiotic islands

Medicago proteins associated with symbiotic islands as defined by Pecrix et al. [41], were blasted using blastp against *Lotus* Gifu proteins annotated in the present assembly, and the best hit was extracted. It was then determined if there was microsynteny between the *Medicago* genes in the symbiotic island and the best *Lotus* matches (**Supplemental file 5**). *M. truncatula* RNA-seq data (**Supplemental table 2**) was trimmed using trimmomatic (10.1093/bioinformatics/btu170), trimmed reads were mapped to the *Medicago truncatula* v.5 reference sequence (MtrunA17r5.0) using the splice aware STAR aligner (version 2.5.1a) [67]. A read was allowed to map in at most 10 locations (–outFilterMultimapNmax 10) with a maximum of 4% mismatches (–outFilterMismatchNoverLmax 0.04) and all non--canonical intron motifs were filtered out (–outFilterIntronMotifs RemoveNoncanonicalUnannotated). In order to obtain non-unique gene-level counts from the mapping files, HTSeq (version 0.9.1) [68] with the 'nonunique all'-method was used. Normalization of read counts was performed by library sequence depth using the R-package DESeq2 (version 1.23.3) [66]. Log expression ratios of 10 dpi nodule samples versus non-inoculated root samples were calculated for *Lotus* and *Medicago* and Pearson correlation coefficients were calculated (**Supplemental tables 1-2**). For calculation of Pearson correlation coefficients, all *Medicago* RNA-seq samples listed in **Supplemental table 2** were used, while *Lotus* root and nodule samples were used (**Supplemental table 1**). When analysing the largest possible set of genes (**Figure 3B**), all

Medicago genes with a match to a *Lotus* gene anywhere in the genome were included along with one *Lotus* match per *Medicago* gene, allowing many copies of the same *Lotus* gene. For analysis of unique *Lotus* genes, only a single *Medicago* gene was included per *Lotus* match within the microsyntenic region and islands with less than three *Lotus* microsyntenic hits were not considered (**Figure 3C**). All statistical analyses were carried out using R v. 3.4.3. The scripts used for analysis are freely available from GitHub (https://github.com/stiguandersen/LotjaGifuGenome).

Data availability

Sequencing data is available from SRA. PacBio data used for genome assembly and Hi-C data from Phase Genomics used for construction of proximity map (PRJNA498060); Illumina paired-end data from RIL resequencing used for genetic map construction (PRJNA498068); RNA-seq data used for annotation (PRJNA622801). Assembly pseudomolecules are available from the NCBI Nucleotide repository with accession numbers AP022629-AP022637. Pseudomolecule sequences and genome annotation information are also found in **Supplemental Files 2 and 3** and are available for browsing and download at *Lotus* Base (https://lotus.au.dk) and LegumeBase (https://www.legumebase.brc.miyazaki-u.ac.jp).

Author contributions

Conceptualization, S.U.A., S.S. and K.F.X.M; Validation, N.K., S.S., K.F.X.M and S.U.A.; Formal Analysis, N.K., T.M., D.R., T.Y.A., T.A., H.H., S.S. and SUA; Investigation, N.S; Resources, J.S., S.S., K.F.X.M., S.U.A.; Data Curation, N.K., S.S., K.F.X.M and S.U.A.; Writing – Original Draft, S.U.A. and N.K.; Writing – Review & Editing, S.U.A. and N.K. with input from all authors; Visualization, N.K., S.U.A. and D.R.; Supervision, S.U.A., S.S. and K.F.X.M.; Project Administration, J.S., S.S., K.F.X.M. and S.U.A.; Funding Acquisition, J.S., S.S., K.F.X.M., S.U.A.

Acknowledgements

The work was supported by the Danish National Research Foundation grant DNRF79 (J.S.), the Genome Information Upgrading Program of the National BioResource Project in 2014 and 2015 (S.S.), a JST CREST grant (number JPMJCR16O1) (S.S.), the CRISBAR grant of the German ministry for education and research (BMBF) (K.F.X.M.) and grant no. 10-081677 from The Danish Council for Independent Research | Technology and Production Sciences (S.U.A.).

Supplemental files

Supplemental file 1: Contig assignment to genetic map segments

Supplemental file 2: *Lotus* Gifu version 1.1 genome sequence

Supplemental file 3: *Lotus* Gifu version 1.2 genome annotation

Supplemental file 4: *Lotus* Gifu expression atlas

Supplemental file 5: *Lotus* Gifu BLAST matches to *Medicago* genes in symbiotic islands

Supplemental file 6: *Medicago* expression data

References

1. Handberg, K., and Stougaard, J. 1992, Lotus japonicus, an autogamous, diploid legume species for classical and molecular genetics. *Plant J.*, **2**, 487–96.
2. Kawaguchi, M., Motomura, T., Imaizumi-Anraku, H., Akao, S., and Kawasaki, S. 2001, Providing the basis for genomics in Lotus japonicus: the accessions Miyakojima and Gifu are appropriate crossing partners for genetic analyses. *Mol. Genet. Genomics*, **266**, 157–66.
3. Kawaguchi, M., Pedrosa-Harand, A., Yano, K., et al. 2005, Lotus burttii takes a position of the third corner in the lotus molecular genetics triangle. *DNA Res.*, **12**, 69–77.
4. Sandal, N., Petersen, T. R., Murray, J., et al. 2006, Genetics of symbiosis in Lotus japonicus: recombinant inbred lines, comparative genetic maps, and map position of 35 symbiotic loci. *Mol. Plant Microbe Interact.*, **19**, 80–91.
5. Oldroyd, G. E. D. 2013, Speak, friend, and enter: signalling systems that promote beneficial symbiotic associations in plants. *Nat. Rev. Microbiol.*, **11**, 252–63.
6. Desbrosses, G. J., and Stougaard, J. 2011, Root nodulation: a paradigm for how plant-microbe symbiosis influences host developmental pathways. *Cell Host Microbe*, **10**, 348–58.
7. Madsen, L. H., Tirichine, L., Jurkiewicz, A., et al. 2010, The molecular network governing nodule organogenesis and infection in the model legume Lotus japonicus. *Nat Commun*, **1**, 10–2.
8. Radutoiu, S., Madsen, L. H., Madsen, E. B., et al. 2003, Plant recognition of symbiotic bacteria requires two LysM receptor-like kinases. *Nature*, **425**, 585–92.

9. Guether, M., Neuhäuser, B., Balestrini, R., Dynowski, M., Ludewig, U., and Bonfante, P. 2009, A mycorrhizal-specific ammonium transporter from Lotus japonicus acquires nitrogen released by arbuscular mycorrhizal fungi. *Plant Physiol.*, **150**, 73–83.
10. Kojima, T., Saito, K., Oba, H., et al. 2014, Isolation and phenotypic characterization of Lotus japonicus mutants specifically defective in arbuscular mycorrhizal formation. *Plant Cell Physiol.*, **55**, 928–41.
11. Rasmussen, S. R., Füchtbauer, W., Novero, M., et al. 2016, Intraradical colonization by arbuscular mycorrhizal fungi triggers induction of a lipochitooligosaccharide receptor. *Sci Rep*, **6**, 29733–12.
12. Webb, K. J., Robbins, M., Wang, T. L., Parniske, M., and Márquez, A. 2005, Mutagenesis In: *Lotus japonicus Handbook*. Springer, Dordrecht, Berlin/Heidelberg, pp. 177–86.
13. Shah, N., Wakabayashi, T., Kawamura, Y., et al. 2020, Extreme genetic signatures of local adaptation during Lotus japonicus colonization of Japan. *Nat Commun*, **11**, 253–15.
14. Sandal, N., Jin, H., Rodríguez-Navarro, D.-N., et al. 2012, A set of Lotus japonicus Gifu x Lotus burttii recombinant inbred lines facilitates map-based cloning and QTL mapping. *DNA Res.*, **19**, 317–23.
15. Shah, N., Hirakawa, H., Kusakabe, S., et al. 2016, High-resolution genetic maps of Lotus japonicus and L. burttii based on re-sequencing of recombinant inbred lines. *DNA Res.*, **23**, 487–94.
16. Perry, J. A., Wang, T. L., Welham, T. J., et al. 2003, A TILLING Reverse Genetics Tool and a Web-Accessible Collection of Mutants of the Legume Lotus japonicus. *Plant Physiol.*, **131**, 866–71.
17. Fukai, E., Soyano, T., Umehara, Y., et al. 2012, Establishment of a Lotus japonicus gene tagging population using the exon-targeting endogenous retrotransposon LORE1. *Plant J.*, **69**, 720–30.
18. Małolepszy, A., Mun, T., Sandal, N., et al. 2016, The LORE1 insertion mutant resource. *Plant J.*, **88**, 306–17.
19. Urbański, D. F., Małolepszy, A., Stougaard, J., and Andersen, S. U. 2012, Genome-wide LORE1 retrotransposon mutagenesis and high-throughput insertion detection in Lotus japonicus. *Plant J.*, **69**, 731–41.
20. Díaz, P., Betti, M., Sanchez, D. H., Udvardi, M. K., Monza, J., and Marquez, A. J. 2010, Deficiency in plastidic glutamine synthetase alters proline metabolism and transcriptomic response in Lotus japonicus under drought stress. *New Phytol.*, **188**, 1001–13.
21. Giovannetti, M., Mari, A., Novero, M., and Bonfante, P. 2015, Early Lotus japonicus root transcriptomic responses to symbiotic and pathogenic fungal exudates. *Front Plant Sci*, **6**, 480.
22. Guether, M., Balestrini, R., Hannah, M., He, J., Udvardi, M. K., and Bonfante, P. 2009, Genome-wide reprogramming of regulatory networks, transport, cell wall and membrane biogenesis during arbuscular mycorrhizal symbiosis in Lotus japonicus. *New Phytol.*, **182**, 200–12.
23. Handa, Y., Nishide, H., Takeda, N., Suzuki, Y., Kawaguchi, M., and Saito, K. 2015, RNA-seq Transcriptional Profiling of an Arbuscular Mycorrhiza Provides Insights into Regulated and Coordinated Gene Expression in Lotus japonicus and Rhizophagus irregularis. *Plant Cell Physiol.*, **56**, 1490–511.
24. Høgslund, N., Radutoiu, S., Krusell, L., et al. 2009, Dissection of symbiosis and organ development by integrated transcriptome analysis of lotus japonicus mutant and wild-type plants. Provart, N. J., (ed.). *PLoS ONE*, **4**, e6556.
25. Kelly, S., Mun, T., Stougaard, J., Ben, C., and Andersen, S. U. 2018, Distinct Lotus japonicus Transcriptomic Responses to a Spectrum of Bacteria Ranging From Symbiotic to Pathogenic. *Front Plant Sci*, **9**, 1218.
26. Munch, D., Gupta, V., Bachmann, A., et al. 2018, The Brassicaceae Family Displays Divergent, Shoot-Skewed NLR Resistance Gene Expression. *Plant Physiol.*, **176**, 1598–609.

27. Sanchez, D. H., Lippold, F., Redestig, H., et al. 2008, Integrative functional genomics of salt acclimatization in the model legume Lotus japonicus. *Plant J.*, **53**, 973–87.
28. Sasaki, T., Suzaki, T., Soyano, T., Kojima, M., Sakakibara, H., and Kawaguchi, M. 2014, Shoot-derived cytokinins systemically regulate root nodulation. *Nat Commun*, **5**, 4983–9.
29. Suzaki, T., Ito, M., Yoro, E., et al. 2014, Endoreduplication-mediated initiation of symbiotic organ development in Lotus japonicus. *Development*, **141**, 2441–5.
30. Verdier, J., Torres-Jerez, I., Wang, M., et al. 2013, Establishment of the Lotus japonicus Gene Expression Atlas (LjGEA) and its use to explore legume seed maturation. *Plant J.*, **74**, 351–62.
31. Mun, T., Bachmann, A., Gupta, V., Stougaard, J., and Andersen, S. U. 2016, Lotus Base: An integrated information portal for the model legume Lotus japonicus. *Sci Rep*, **6**, 39447.
32. Ito, M., Miyamoto, J., Mori, Y., et al. 2000, Genome and Chromosome Dimensions of Lotus japonicus. *J Plant Res*, **113**, 435–42.
33. Tabata, S., and Stougaard, J. (eds.). 2014, *The Lotus japonicus Genome*. Springer Berlin Heidelberg, Berlin, Heidelberg.
34. Sato, S., Nakamura, Y., Kaneko, T., et al. 2008, Genome Structure of the Legume, Lotus japonicus. *DNA Res.*, **15**, 227–39.
35. Luo, R., Liu, B., Xie, Y., et al. 2012, SOAPdenovo2: an empirically improved memory-efficient short-read de novo assembler. *Gigascience*, **1**, 18.
36. Huang, X., Wang, J., Aluru, S., Yang, S.-P., and Hillier, L. 2003, PCAP: a whole-genome assembly program. *Genome Res.*, **13**, 2164–70.
37. Fukai, E., Umehara, Y., Sato, S., et al. 2010, Derepression of the plant Chromovirus LORE1 induces germline transposition in regenerated plants. Schnable, P. S., (ed.). *PLoS Genet.*, **6**, e1000868.
38. Hayashi, M., Miyahara, A., Sato, S., et al. 2001, Construction of a Genetic Linkage Map of the Model Legume Lotus japonicus Using an Intraspecific F 2 Population. *DNA Res.*, **8**, 301–10.
39. Pedrosa, A., Sandal, N., Stougaard, J., Schweizer, D., and Bachmair, A. 2002, Chromosomal Map of the Model Legume Lotus japonicus. *Genetics*, **161**, 1661–72.
40. Roy, S., Liu, W., Nandety, R. S., et al. 2020, Celebrating 20 Years of Genetic Discoveries in Legume Nodulation and Symbiotic Nitrogen Fixation. *Plant Cell*, **32**, 15–41.
41. Pecrix, Y., Staton, S. E., Sallet, E., et al. 2018, Whole-genome landscape of Medicago truncatula symbiotic genes. *Nat Plants*, **356**, eaad4501.
42. Koren, S., Walenz, B. P., Berlin, K., Miller, J. R., Bergman, N. H., and Phillippy, A. M. 2017, Canu: scalable and accurate long-read assembly via adaptive k-mer weighting and repeat separation. *Genome Res.*, **27**, 722–36.
43. Ohmido, N., Ishimaru, A., Kato, S., Sato, S., Tabata, S., and Fukui, K. 2010, Integration of cytogenetic and genetic linkage maps of Lotus japonicus, a model plant for legumes. *Chromosome Res.*, **18**, 287–99.
44. Simão, F. A., Waterhouse, R. M., Ioannidis, P., Kriventseva, E. V., and Zdobnov, E. M. 2015, BUSCO: assessing genome assembly and annotation completeness with single-copy orthologs. *Bioinformatics*, **31**, 3210–2.
45. Tomato Genome Consortium. 2012, The tomato genome sequence provides insights into fleshy fruit evolution. *Nature*, **485**, 635–41.
46. Schauser, L., Roussis, A., Stiller, J., and Stougaard, J. 1999, A plant regulator controlling development of symbiotic root nodules. *Nature*, **402**, 191–5.
47. Tirichine, L., Imaizumi-Anraku, H., Yoshida, S., et al. 2006, Deregulation of a Ca2+/calmodulin-dependent kinase leads to spontaneous nodule development. *Nature*, **441**, 1153–6.
48. Yano, K., Yoshida, S., Müller, J., et al. 2008, CYCLOPS, a mediator of symbiotic intracellular accommodation. *Proc. Natl. Acad. Sci. U.S.A.*, **105**, 20540–5.
49. Schmutz, J., Cannon, S. B., Schlueter, J., et al. 2010, Genome sequence of the palaeopolyploid soybean. *Nature*, **463**, 178–83.

50. Kereszt, A., Mergaert, P., Montiel, J., Endre, G., and Kondorosi, É. 2018, Impact of Plant Peptides on Symbiotic Nodule Development and Functioning. *Front Plant Sci*, **9**, 1026.
51. Zhang, H.-B., Zhao, X., Ding, X., Paterson, A. H., and Wing, R. A. 1995, Preparation of megabase-size DNA from plant nuclei. *Plant J.*, **7**, 175–84.
52. Li, H., and Durbin, R. 2009, Fast and accurate short read alignment with Burrows-Wheeler transform. *Bioinformatics*, **25**, 1754–60.
53. Li, H., Handsaker, B., Wysoker, A., et al. 2009, The Sequence Alignment/Map format and SAMtools. *Bioinformatics*, **25**, 2078–9.
54. Lieberman-Aiden, E., van Berkum, N. L., Williams, L., et al. 2009, Comprehensive mapping of long-range interactions reveals folding principles of the human genome. *Science*, **326**, 289–93.
55. Bickhart, D. M., Rosen, B. D., Koren, S., et al. 2017, Single-molecule sequencing and chromatin conformation capture enable de novo reference assembly of the domestic goat genome. *Nat. Genet.*, **49**, 643–50.
56. Burton, J. N., Adey, A., Patwardhan, R. P., Qiu, R., Kitzman, J. O., and Shendure, J. 2013, Chromosome-scale scaffolding of de novo genome assemblies based on chromatin interactions. *Nat. Biotechnol.*, **31**, 1119–25.
57. Gremme, G., Brendel, V., Sparks, M. E., and Kurtz, S. 2005, Engineering a software tool for gene structure prediction in higher organisms. *Information and Software Technology*, **47**, 965–78.
58. Kim, D., Paggi, J. M., Park, C., Bennett, C., and Salzberg, S. L. 2019, Graph-based genome alignment and genotyping with HISAT2 and HISAT-genotype. *Nat. Biotechnol.*, **37**, 907–15.
59. Pertea, M., Pertea, G. M., Antonescu, C. M., Chang, T.-C., Mendell, J. T., and Salzberg, S. L. 2015, StringTie enables improved reconstruction of a transcriptome from RNA-seq reads. *Nat. Biotechnol.*, **33**, 290–5.
60. Altschul, S. F., Gish, W., Miller, W., Myers, E. W., and Lipman, D. J. 1990, Basic local alignment search tool. *J. Mol. Biol.*, **215**, 403–10.
61. Eddy, S. R. 2011, Accelerated Profile HMM Searches. Pearson, W. R., (ed.). *PLoS Comput Biol*, **7**, e1002195.
62. Lowe, T. M., and Eddy, S. R. 1997, tRNAscan-SE: a program for improved detection of transfer RNA genes in genomic sequence. *Nucleic Acids Res.*, **25**, 955–64.
63. Lagesen, K., Hallin, P., Rødland, E. A., Staerfeldt, H.-H., Rognes, T., and Ussery, D. W. 2007, RNAmmer: consistent and rapid annotation of ribosomal RNA genes. *Nucleic Acids Res.*, **35**, 3100–8.
64. Nawrocki, E. P., and Eddy, S. R. 2013, Infernal 1.1: 100-fold faster RNA homology searches. *Bioinformatics*, **29**, 2933–5.
65. Patro, R., Duggal, G., Love, M. I., Irizarry, R. A., and Kingsford, C. 2017, Salmon provides fast and bias-aware quantification of transcript expression. *Nat. Methods*, **14**, 417–9.
66. Love, M. I., Huber, W., and Anders, S. 2014, Moderated estimation of fold change and dispersion for RNA-seq data with DESeq2. *Genome Biol.*, **15**, 550–21.
67. Dobin, A., Davis, C. A., Schlesinger, F., et al. 2013, STAR: ultrafast universal RNA-seq aligner. *Bioinformatics*, **29**, 15–21.
68. Anders, S., Pyl, P. T., and Huber, W. 2015, HTSeq--a Python framework to work with high-throughput sequencing data. *Bioinformatics*, **31**, 166–9.

Figures

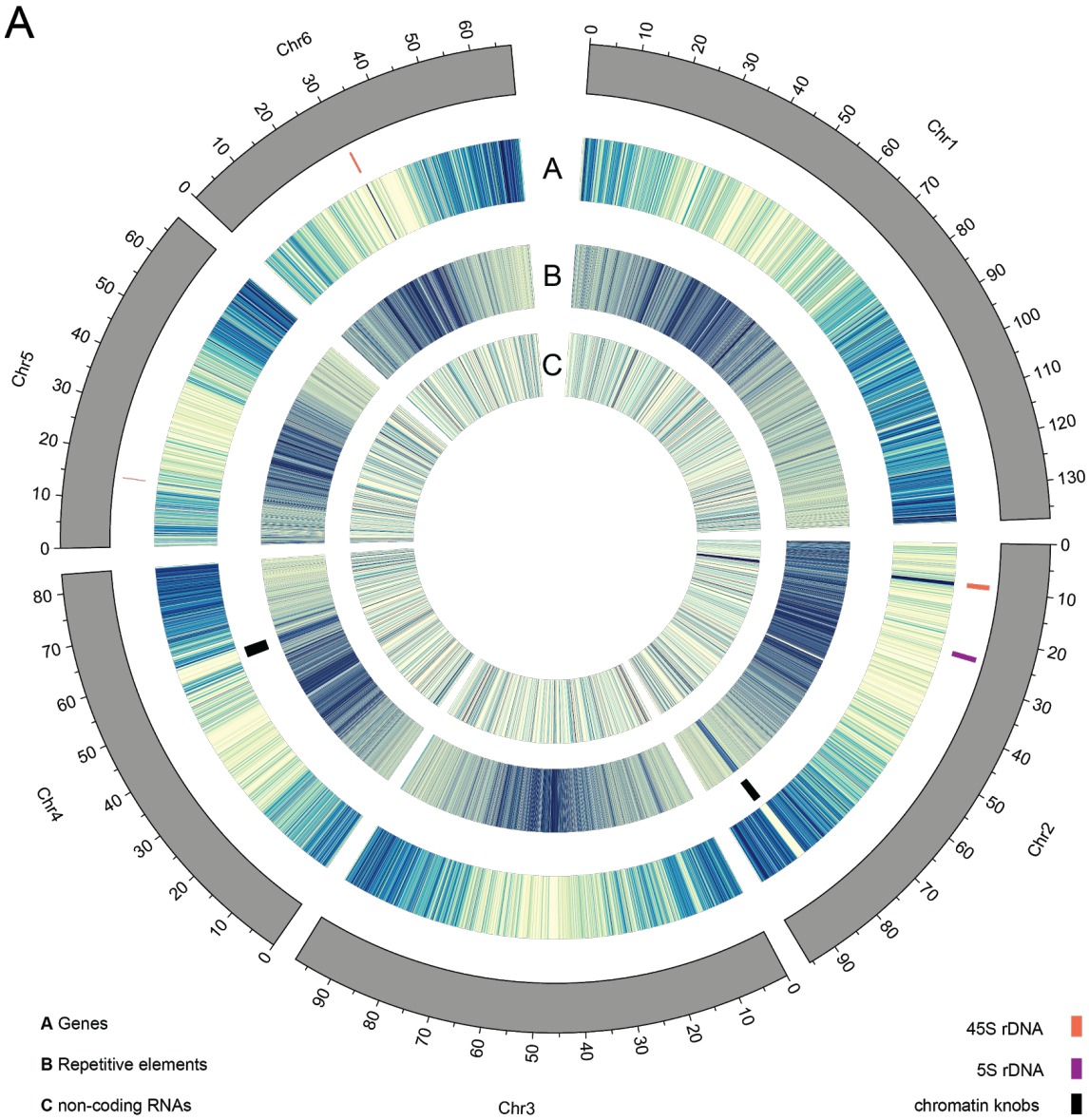
A
Chr1
Chr2
Chr3
Chr4
Chr5
Chr6
A
B
C
A Genes
B Repetitive elements
C non-coding RNAs
45S rDNA
5S rDNA
chromatin knobs

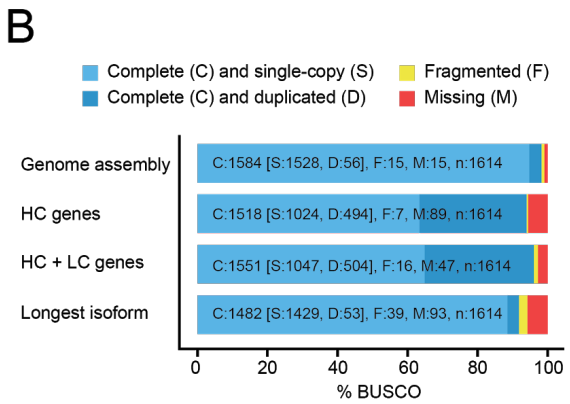
B
Complete (C) and single-copy (S)
Complete (C) and duplicated (D)
Fragmented (F)
Missing (M)
Genome assembly
C:1584 [S:1528, D:56], F:15, M:15, n:1614
HC genes
C:1518 [S:1024, D:494], F:7, M:89, n:1614
HC + LC genes
C:1551 [S:1047, D:504], F:16, M:47, n:1614
Longest isoform
C:1482 [S:1429, D:53], F:39, M:93, n:1614
% BUSCO

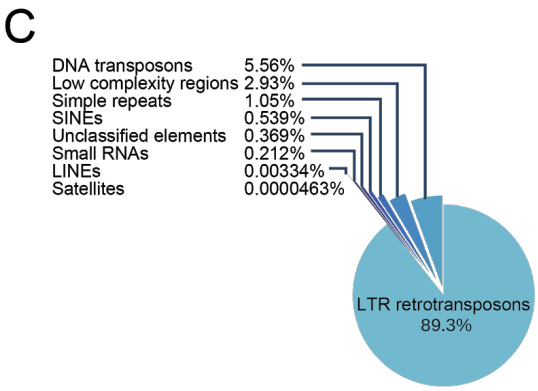
C
DNA transposons 5.56%
Low complexity regions 2.93%
Simple repeats 1.05%
SINEs 0.539%
Unclassified elements 0.369%
Small RNAs 0.212%
LINEs 0.00334%
Satellites 0.0000463%
LTR retrotransposons
89.3%

Figure 1: **A**) Circos diagram displaying heatmaps of the numbers of genes and ncRNAs (100 Mb bins) and bases covered by repetitive elements (10 Mb bins) in the *Lotus* Gifu genome. **B**) BUSCO v4 scores of the *Lotus* Gifu assembly (98.2%), the high confidence gene set (94%), the high- and low confidence gene set (96.1%) and of only the longest transcript of each gene (91.8%) from the joint high and low confidence gene set. Lineage used: embryophyta_odb10. **C**) Distribution of repetitive elements in the *Lotus* Gifu genome.

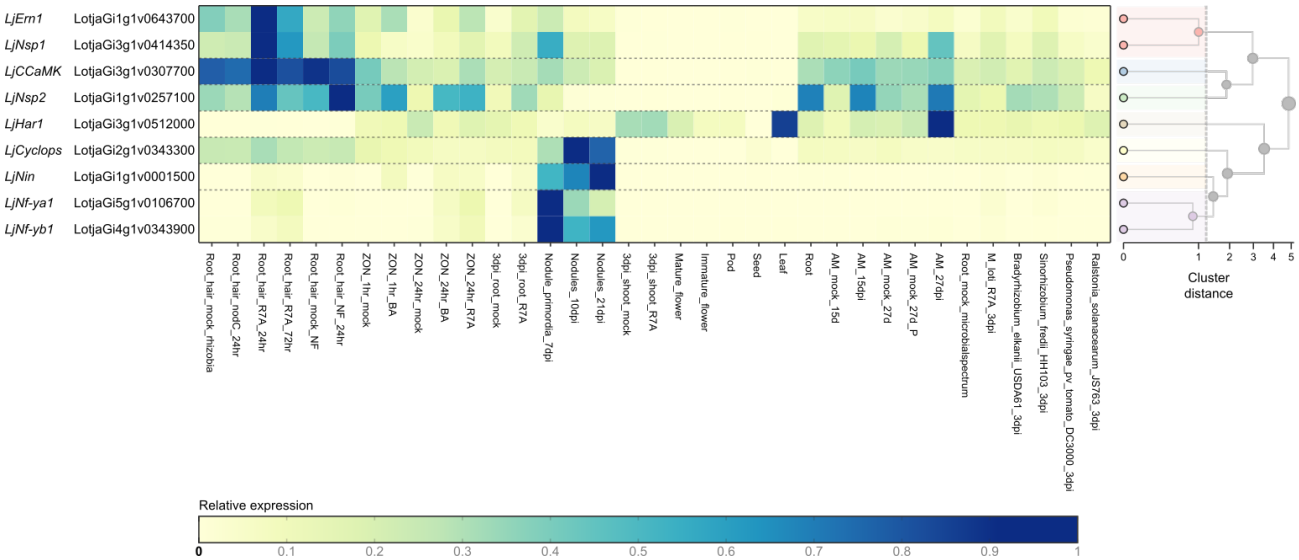

Figure 2. Expression profiles of known symbiosis genes. Expression values from the *Lotus* Gifu RNA-seq expression atlas are shown for the indicated genes. A full description of the conditions included is shown in **Supplemental table 1**. The heatmap was generated from https://lotus.au.dk/expat/ using the normalise by row function.

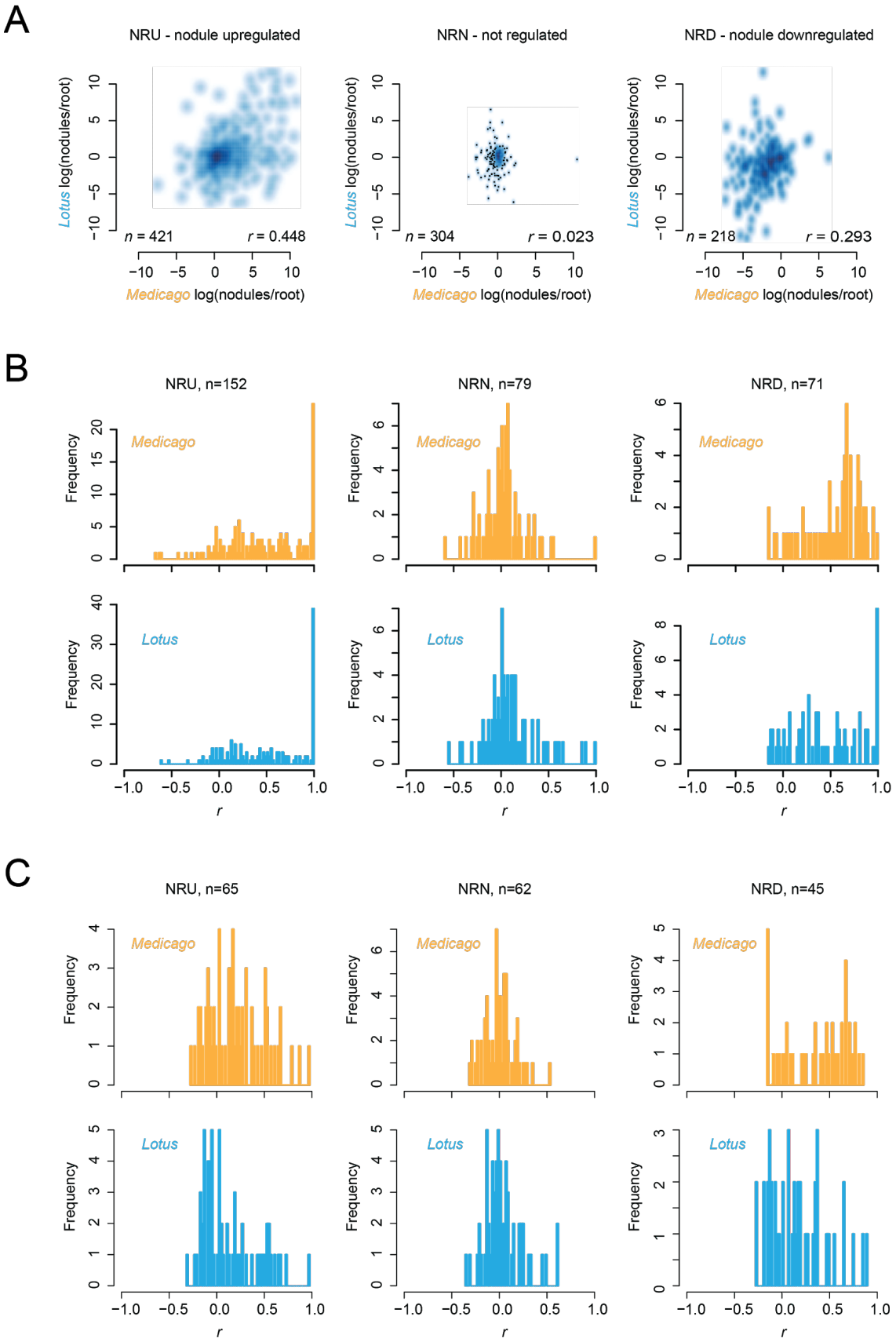
A
NRU - nodule upregulated
NRN - not regulated
NRD - nodule downregulated
Lotus log(nodules/root)
Medicago log(nodules/root)
n = 421
r = 0.448
n = 304
r = 0.023
n = 218
r = 0.293
B
NRU, n=152
NRN, n=79
NRD, n=71
Medicago
Lotus
Frequency
r
C
NRU, n=65
NRN, n=62
NRD, n=45
Medicago
Lotus
Frequency
r

Figure 3: Symbiotic island gene expression. **A)** Log(nodule/root) expression ratios for genes in *Medicago* symbiotic islands and their best *Lotus* blast matches. *n*: gene count. *r*: Pearson correlation coefficient for the *Lotus* and *Medicago* log(nodule/root) ratios. **B-C)** Histograms of Pearson correlation coefficients for symbiotic islands. The Pearson correlation coefficient for each island is an average of the coefficients resulting from pairwise comparisons of the gene expression profiles of all genes residing within that island. *n*: symbiotic island count. **B)** All genes in *Medicago* symbiotic islands with a putative *Lotus* homolog with expression data. Multiple copies of the same *Lotus* gene are allowed. **C)** Only one *Lotus* copy and one corresponding *Medicago* gene is included in the analysis and it is further required that each *Lotus* island contains at least three members. *Lotus*: expression data from *Lotus*. *Medicago*: expression data from *Medicago.*

Tables

Assembly size (Mb)	554.1
Contig count	1685
Contig N50 (Kb)	807
Contig L50	188
Median coverage	73

Table 1. Assembly statistics.

Dataset	Contig count	Total length	N50	L50
Polished assembly	1,686	554,078,227	807,552	187
Containing ≥1 SNP	1,538 (91.2%)	551,215,263 (99.5%)	823,414	185
Exclusively Gifu×*L. burttii*	105 (6.3%)	3,270,218 (0.6%)	35,963	27
Exclusively Gifu×MG-20	124 (7.4%)	5,010,333 (0.9%)	51,370	29
Contains SNP from both	1,309 (77.6%)	542,934,712 (97.9%)	835,713	180
Does not contain any SNP	148 (8.8%)	2,862,964 (0.5%)	23,531	46

Table 2. Contigs from the Gifu assembly after analysing SNPs derived from Gifu×*L. burtii* and Gifu×MG-20 RIL populations.

	Lotus **Gifu v.1.2 HC+LC**	***Lotus*** **Gifu v.1.2 HC**	***Medicago*** **A17 v.4**	***Medicago*** **A17 v.4 HC**	***Medicago*** **A17 v.5**	***Glycine max*** **Williams 82 v. 2.1**
Number of genes	30,243	21,778	50,444	31,451	51,316	52,872
Number of coding genes	29,554	21,778	50,444	31,451	44,623	52,872
mRNAs	49,868	37,994	57,585	38,175	44,623	86,256
exons	306,545	264,198	267,394	397,385	189,379	560,910
CDSs	262,442	236,845	257,792	376,276	174,461	516,059
Average CDNA lengths	2,566.67	2,599.04	1,312.14	1,766.89	1,508.17	2,032.04
Average CDS lengths	1,216.2	1,385.43	1,038.35	1,272.4	1,017.7	1,350.67
Average exon lengths	417.54	373.77	282.58	261.92	360.25	312.48
Average intron lengths	527.12	513.71	444.41	438.41	476.57	519.19
Average transcripts per gene	1.65	1.74	1.14	1.54	1	1.63
Average exons per transcript	6.15	6.95	4.64	6.75	4.19	6.5
Average CDS exons per transcript	5.23	6.23	4.48	6.39	3.91	5.98

Table 3: Statistics of the *Lotus japonicus* Gifu genome annotation in comparison to the *Medicago truncatula* A17 versions 4 and 5, and *Glycine max* v2.1 genome annotations. HC: high confidence gene models. LC: low confidence gene models.

Island type	NRU	NRD	NRN	NDA	NDD	NDN
Islands	270	89	84	49	211	57
Mt genes	2559	712	628	377	1680	429
Mt genes with Lj Gifu hits	1040	550	516	298	506	322
Corresponding Lj Gifu genes	770	358	456	261	396	275
Lj Gifu genes with micro-synteny	446	228	320	190	215	166
Mt lncRNAs	302	40	17	25	228	18
Mt lncRNAs with Lj Gifu hit	47	17	9	13	31	6
Mt lncRNAs with Lj Gifu hit in micro-syntenic region	17	3	5	9	8	5
Conservation rate (%)	40.6%	77.2%	82.2%	79.0%	30.1%	75.1%
Duplication rate	1.35	1.54	1.13	1.14	1.28	1.17
Ratio of genes with micro-synteny	57.9%	63.7%	70.2%	72.8%	54.3%	60.4%
Islands with Lj Gifu hits in more than half of the genes	101 (37%)	80 (90%)	82 (98%)	44 (90%)	36 (17%)	49 (86%)

Table 4. Conservation of symbiotic islands between *Lotus* and *Medicago*. NRU: Nodule vs. root upregulated. NRD: Nodule vs. root downregulated. NRN: Nodule vs. root not regulated. NDA: nodule development apical zone. NDD: Nodule development differentiation zone. NDN: Nodule development not regulated.

Supplemental tables

Tissue	Sample name	Nod regulation	Correlation	Replicates	Reference	Bioproject ID
Root susceptible zone	ZON_1hr_mock			3	Current study	PRJNA622396
Root susceptible zone	ZON_1hr_BA			3	Current study	PRJNA622396
Root susceptible zone	ZON_24hr_mock			3	Current study	PRJNA622396
Root susceptible zone	ZON_2 hr_BA			3	Current study	PRJNA622396
Root susceptible zone	ZON_24hr_R7A			3	Current study	PRJNA622396
Nodule	nodules_10dpi	x	x	3	Current study	PRJNA622396
Root	3dpi_root_mock	x	x	3	Munch et al 2017	PRJNA384655
Root	3dpi_root_R7A		x	3	Munch et al 2017	PRJNA384655
Shoot	3dpi_shoot_mock			3	Munch et al 2017	PRJNA384655
Shoot	3dpi_shoot_R7A			3	Munch et al 2017	PRJNA384655
Flower	Mature_flower			3	NIBB	PRJDB2436
Flower	Immature_flower			3	NIBB	PRJDB2436
Pod	Pod			3	NIBB	PRJDB2436
Seed	seed			3	NIBB	PRJDB2436
Root	root		x	3	NIBB	PRJDB2436
Leaf	leaf			3	NIBB	PRJDB2436
Root	AM_15dpi			3	Handa et al 2015	PRJDB2819, PRJDB2576, PRJDB3212
Root	AM_27dpi			3	Handa et al 2015	PRJDB2819, PRJDB2576, PRJDB3212
Root	AM_mock_15d			3	Handa et al 2015	PRJDB2819, PRJDB2576, PRJDB3212
Root	AM_mock_27d_ P			3	Handa et al 2015	PRJDB2819, PRJDB2576, PRJDB3212
Root	AM_mock_27			3	Handa et al 2015	PRJDB2819, PRJDB2576, PRJDB3212
Root hair	root_hair_mock_rhizobia			3	Kelly et al 2018	PRJNA422278
Root hair	root_hair_nodC_24h			3	Kelly et al 2018	PRJNA422278
Root hair	root_hair_R7A_24hr			3	Kelly et al 2018	PRJNA422278
Root hair	root_hair_R7A_72hr			3	Kelly et al 2018	PRJNA422278
Root hair	root_hair_mock_NF			3	Kelly et al 2018	PRJNA422278
Root hair	root_hair_NF_24hr			3	Kelly et al 2018	PRJNA422278
Nodule	nodule_primordia_7_dpi		x	3	Kelly et al 2018	PRJNA422278
Nodule	nodules_21dpi		x	1	Kelly et al 2018	PRJNA422278
Root	Root_mock_microbialspectrum		x	2	Kelly et al 2018	PRJNA422278
Root	M_loti_R7A_3dpi		x	2	Kelly et al 2018	PRJNA422278
Root	Bradyrhizobium_elkanii_USDA61_3dpi			2	Kelly et al 2018	PRJNA422278
Root	Sinorhizobium_fredii_HH103_3dpi			2	Kelly et al 2018	PRJNA422278
Root	Pseudomonas_syringae_pv_tomato_DC3000_3dpi			2	Kelly et al 2018	PRJNA422278
Root	Ralstonia_solanacearum_JS763_3dpi			2	Kelly et al 2018	PRJNA422278

Supplemental table 1. *Lotus* Gifu RNA-seq samples. Nod regulation: Samples used for calculating expression differences between roots and nodules. Correlation: Samples used for calculating Pearson correlation coefficients for gene expression co-regulation in symbiotic islands. NIBB: National Institute for Basic Biology, Japan. References: **Handa** Y, Nishide H, Takeda N, Suzuki Y, Kawaguchi M, Saito K. RNA-seq Transcriptional Profiling of an Arbuscular Mycorrhiza Provides Insights into Regulated and Coordinated Gene Expression in Lotus japonicus and Rhizophagus irregularis. Plant Cell Physiol. 2015 Aug;56(8):1490–511. **Kelly** S, Mun T, Stougaard J, Ben C, Andersen SU. Distinct Lotus japonicus Transcriptomic Responses to a Spectrum of Bacteria Ranging From Symbiotic to Pathogenic. Front Plant Sci. 2018;9:1218. **Munch** D, Gupta V, Bachmann A, Busch W, Kelly S, Mun T, et al. The Brassicaceae Family Displays Divergent, Shoot-Skewed NLR Resistance Gene Expression. Plant Physiol. American Society of Plant Biologists; 2018 Feb;176(2):1598–609.

SRA Sample ID	Sample Name	Tissue	Treatment
SRR5740859	MtNod0dpi_1	Roots	Non-inoculated
SRR5740858	MtNod0dpi_2	Roots	Non-inoculated
SRR5740868	MtNod0dpi_3	Roots	Non-inoculated
SRR5740875	MtNod4dpi_1	Roots	4 days post inoculation with *S. meliloti* 1021
SRR5740878	MtNod4dpi_2	Roots	4 days post inoculation with *S. meliloti* 1021
SRR5740877	MtNod4dpi_3	Roots	4 days post inoculation with *S. meliloti* 1021
SRR5740870	MtNod10dpi_1	Nodules	10 days post inoculation with *S. meliloti* 1021
SRR5740864	MtNod10dpi_2	Nodules	10 days post inoculation with *S. meliloti* 1021
SRR5740861	MtNod10dpi_3	Nodules	10 days post inoculation with *S. meliloti* 1021
SRR5740862	MtNod14dpi_1	Nodules	14 days post inoculation with *S. meliloti* 1021
SRR5740866	MtNod14dpi_2	Nodules	14 days post inoculation with *S. meliloti* 1021
SRR5740869	MtNod14dpi_3	Nodules	14 days post inoculation with *S. meliloti* 1021
SRR5740860	MtNod14dpi_12h_1	Nodules	14 days post inoculation with *S. meliloti* 1021, 12h nitrogen treatment
SRR5740871	MtNod14dpi_12h_2	Nodules	14 days post inoculation with *S. meliloti* 1021, 12h nitrogen treatment
SRR5740874	MtNod14dpi_12h_3	Nodules	14 days post inoculation with *S. meliloti* 1021, 12h nitrogen treatment
SRR5740873	MtNod14dpi_48h_1	Nodules	14 days post inoculation with *S. meliloti* 1021, 48h nitrogen treatment
SRR5740872	MtNod14dpi_48h_2	Nodules	14 days post inoculation with *S. meliloti* 1021, 48h nitrogen treatment
SRR5740876	MtNod14dpi_48h_3	Nodules	14 days post inoculation with S. meliloti 1021, 48h nitrogen treatment
SRR5740867	Mt4wkNod_1	Nodules	4 weeks post inoculation with *S. meliloti* 1021
SRR5740865	Mt4wkNod_2	Nodules	4 weeks post inoculation with *S. meliloti* 1021
SRR5740863	Mt4wkNod_3	Nodules	4 weeks post inoculation with *S. meliloti* 1021

Supplemental table 2. *Medicago truncatula* RNA-seq data. SRA: Sequence read archive (https://www.ncbi.nlm.nih.gov/sra).

NRU islands	*r Medicago*	*r Lotus*	Island size	log(nodules/root) *Lotus*	log(root/nodules) *Medicago*
SRI_NRU0026	0.53	0.97	3	11.37	7.49
SRI_NRU0105	0.12	0.72	3	-2.28	1.73
SRI_NRU0009	-0.17	0.67	3	-2.80	-0.96
SRI_NRU0016	0.52	0.66	3	3.73	3.33
SRI_NRU0032	-0.07	0.61	3	-1.54	1.93
SRI_NRU0093	0.16	0.57	4	1.34	2.70
SRI_NRU0209	0.26	0.55	3	4.25	0.98
SRI_NRU0103	0.25	0.54	6	2.81	1.55
SRI_NRU0059	0.52	0.53	3	6.15	3.31
SRI_NRU0005	0.04	0.52	6	-1.07	0.36
SRI_NRU0170	0.60	0.52	3	-0.91	2.30
SRI_NRU0143	0.31	0.49	3	0.55	0.80
SRI_NRU0246	-0.11	0.47	3	-1.13	-0.13
SRI_NRU0139	0.23	0.44	3	-0.40	0.12
SRI_NRU0156	0.32	0.43	4	-1.03	3.05
SRI_NRU0089	0.21	0.38	5	1.20	0.69
SRI_NRU0207	0.66	0.31	4	2.81	3.96
SRI_NRU0058	0.96	0.28	3	3.29	3.50
SRI_NRU0019	0.66	0.27	3	-0.81	-2.07
SRI_NRU0003	0.05	0.25	3	-2.41	1.09

Supplemental table 3. Top correlated NRU islands. The table is sorted by the *Lotus* correlation coefficient (*r*). *r*: average Pearson correlation coefficient for pairwise comparisons of gene expression profiles. Island size: number of genes within each island.

NRN islands	*r Medicago*	*r Lotus*	Island size	log(nodules/root) *Lotus*	log(root/nodules) *Medicago*
SRI_NRN0005	0.19	0.62	3	-0.65	0.09
SRI_NRN0060	0.14	0.61	4	-0.96	-0.74
SRI_NRN0021	-0.18	0.49	3	-0.73	0.90
SRI_NRN0034	0.04	0.46	3	0.16	-0.44
SRI_NRN0028	0.18	0.33	5	0.20	0.66
SRI_NRN0068	0.06	0.31	5	-0.24	-0.12
SRI_NRN0074	-0.31	0.26	3	-1.49	-0.40
SRI_NRN0044	0.19	0.24	3	-0.46	0.26
SRI_NRN0013	-0.04	0.23	8	0.34	-0.06
SRI_NRN0075	-0.03	0.23	3	0.53	0.10
SRI_NRN0018	0.04	0.21	7	0.19	-0.15
SRI_NRN0014	0.02	0.20	3	0.74	4.06
SRI_NRN0016	0.07	0.15	4	-1.13	-0.66
SRI_NRN0035	0.19	0.14	4	-0.22	0.14
SRI_NRN0051	0.06	0.12	5	0.09	-0.03
SRI_NRN0038	0.00	0.10	7	-0.16	0.30
SRI_NRN0030	0.03	0.09	3	0.51	0.13
SRI_NRN0056	-0.23	0.08	4	0.22	0.08
SRI_NRN0080	-0.14	0.08	4	-0.16	-0.28
SRI_NRN0079	0.07	0.07	4	0.25	-0.08

Supplemental table 4. Top correlated NRN islands. The table is sorted by the *Lotus* correlation coefficient (*r*). *r*: average Pearson correlation coefficient for pairwise comparisons of gene expression profiles. Island size: number of genes within each island.

NRD islands	*r Medicago*	*r Lotus*	Island size	log(nodules/root) *Lotus*	log(root/nodules) *Medicago*
SRI_NRD0027	0.43	0.88	5	-4.36	-1.63
SRI_NRD0080	0.73	0.85	3	-3.81	-3.36
SRI_NRD0087	0.71	0.74	3	-4.08	-3.30
SRI_NRD0005	-0.15	0.66	3	-3.11	-1.60
SRI_NRD0017	0.71	0.64	4	-2.75	-2.91
SRI_NRD0031	-0.02	0.56	4	-3.45	-2.92
SRI_NRD0047	0.21	0.49	3	-2.70	-0.49
SRI_NRD0046	0.85	0.47	3	-3.68	-4.92
SRI_NRD0045	0.82	0.37	3	-4.01	-3.62
SRI_NRD0019	0.01	0.36	3	-0.96	-1.55
SRI_NRD0044	0.22	0.36	5	-1.47	-2.56
SRI_NRD0034	-0.15	0.34	4	-0.84	-0.63
SRI_NRD0043	0.77	0.34	3	2.30	-1.35
SRI_NRD0042	0.47	0.33	5	-2.16	-1.15
SRI_NRD0072	0.49	0.28	4	-0.86	-3.09
SRI_NRD0007	0.35	0.26	6	-1.58	-1.83
SRI_NRD0006	0.67	0.20	3	1.55	-2.10
SRI_NRD0056	-0.05	0.20	4	-2.78	-1.73
SRI_NRD0024	0.55	0.17	4	2.99	-2.93
SRI_NRD0054	0.63	0.16	3	-0.94	-1.65

Supplemental table 5. Top correlated NRD islands. The table is sorted by the *Lotus* correlation coefficient (*r*). *r*: average Pearson correlation coefficient for pairwise comparisons of gene expression profiles. Island size: number of genes within each island.

gene ID	chromosome	start	end	strand
LotjaGi2g1v0394950	chr2	89244457	89246244	-
LotjaGi2g1v0440600	chr2	93688296	93690318	+
LotjaGi3g1v0414350	chr3	81961144	81962772	-
LotjaGi3g1v0449330	chr3	86285726	86285971	+
LotjaGi3g1v0449360	chr3	86294832	86295050	+
LotjaGi4g1v0376650	chr4	75571048	75571728	+
LotjaGi5g1v0359230	chr5	67390287	67391829	+
LotjaGi5g1v0359260	chr5	67393483	67394919	+
LotjaGi5g1v0359300	chr5	67400904	67402147	+
LotjaGi5g1v0359350	chr5	67402703	67404660	-

Supplemental table 6. Manually curated genes.